Physics Letters A 448 (2022) 128332

Contents lists available at ScienceDirect

Physics Letters A

www.elsevier.com/locate/pla

Quantum uncertainty: $\Delta x \Delta p$ experimental evaluation and direct visualization

M. Fernández Guasti

Lab. de Óptica Cuántica, Depto. de Física, Universidad A. Metropolitana - Iztapalapa, 09340 México D.F., Ap. Postal. 55-534, Mexico

ARTICLE INFO

Article history:
Received 6 May 2022
Received in revised form 6 July 2022
Accepted 18 July 2022
Available online 22 July 2022
Communicated by M.G.A. Paris

Keywords:
Quantum foundations
Uncertainty measurements
Heisenberg principle
Wave mechanics

ABSTRACT

The intrinsic quantum uncertainty between conjugate observables is a hallmark of quantum theory. Heisenberg's uncertainty has been experimentally tested in elementary particles, molecules and microscopic objects. Uncertainties obtained from diffraction setups have the drawback that position and momentum are measured at different times in dissimilar regions. Joint measurements with alternative setups, have been performed with other complementary variables. A quantum optical realization of the position - linear momentum uncertainty in the quantum limit is presented here. The interference of two non-collinear photon modes with different frequencies are space and time resolved. Detection is performed in the same space-time region, thus achieving a joint measurement. Evaluation of the photon momentum from the position versus time interferograms, makes this procedure akin to the mechanical momentum construct. The obstruction that the position precision imposes on the momentum determination is directly visualized. The measured uncertainties $\Delta x\,\Delta p_x \sim 2\hbar$, consistent with Hesienberg's principle, discern between two theoretical proposals.

1. Introduction

The position and momentum of a particle in the quantum realm cannot be both determined with arbitrary precision. This limitation is not due to the imperfections of the measuring apparatus where more refined devices can produce more accurate results, but an uncertainty that is ever present even with the most sophisticated equipment. But why do these limitations arise and how are they observed? There is an aura of mystery regarding the existence of this uncertainty at a fundamental level in the quantum world but apparently not present in the classical realm. These and other queries have been addressed in diverse publications from the outset of quantum theory, mostly from a theoretical standpoint [1–4].

Formally, Heisenberg's uncertainty principle arises from the non-commutativity between operators representing dynamical variables [5]. The uncertainty relationship establishes the limit with which conjugate variables can be observed $\Delta A \Delta B \geq \frac{1}{2}|\langle AB - BA\rangle|$. The position-momentum uncertainty $\Delta x\,\Delta p_x \geq \frac{\hbar}{2}$ is a consequence of the commutator relation $[\widehat{x}, \widehat{p}_x] = \widehat{x}\widehat{p}_x - \widehat{p}_x\widehat{x} = i\hbar$ between the canonical conjugate position x and momentum p_x observables [6]. $\Delta\Omega \equiv \sqrt{\langle\Omega^2\rangle - \langle\Omega\rangle^2}$ represents the standard deviation of Ω, x or p_x in this case.

Three types of uncertainty relationships are acknowledged: i) Preparation uncertainty relations, constraining the sharpness of the distributions of complementary observables. These measurements are performed on an ensemble of identically prepared quantum systems. ii) Simultaneous measurement relations, involves the product uncertainty of any joint measurement of complementary observables. iii) Measurement - disturbance relations (MDR), where the measurement of one observable alters its complementary pair. The observer's unavoidable disturbance upon measurement becomes of paramount importance. MDR required a reformulation of the uncertainty inequality [7] that has been tested in recent experiments [8–10]. Here we are mainly concerned with i) and ii).

Confirmations of position-momentum Heisenberg's preparation uncertainty have been reported with various particles, for example, diffraction of neutrons [11] and fullerene molecules [12]. Photon diffraction was observed from the outset of quantum theory but is still debated in terms of momentum exchange or classical wave theory [13,14]. However, these experiments do not constitute direct tests of the uncertainty relations in a strict sense; while the position uncertainty is determined by the diffracting slit width, the momentum is inferred from the position distribution at a later time when the particles hit the detection screen [15]. Joint measurements have been reported with different observables other than position and linear momenta, such as the quantum phase [16], amplitude-phase squeezed states [17], the Q-function [18],

E-mail address: mfg@xanum.uam.mx.
URL: https://luz.izt.uam.mx.

https://doi.org/10.1016/j.physleta.2022.128332
0375-9601/

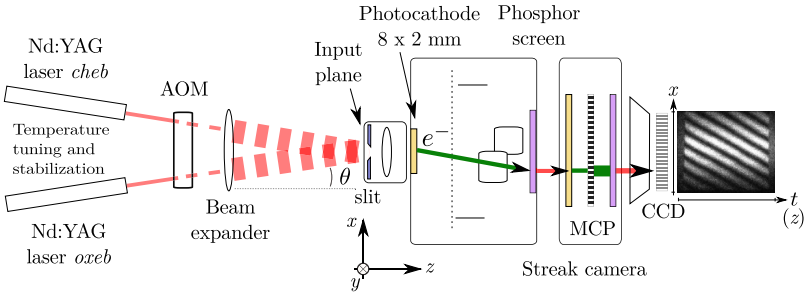

Fig. 1. Schematic diagram of the experimental arrangement. An acousto-optic modulator (AOM) selects 50 ns segments of the two independent CW Nd:YAG monomode lasers. The setup is equivalent to a Young's two slit experiment but each 'slit' is illuminated by an independent laser. The expanded beams overlap at the streak camera input plane, where a variable slit can be used to select the spatial acquisition Δx range. The photons hit the photocathode detector after the input optics de-magnifies the image by 2. The electron beam is swept in the y direction (time axis). A multichannel plate (MCP) is used as image intensifier, an optical fiber tapper couples the light onto a CCD. A two dimensional image is thus acquired that displays the photons density as a function of distance x versus time. (Optical beams drawn in red, electron paths drawn in green.) (For interpretation of the colors in the figure(s), the reader is referred to the web version of this article.)

polarization observables [19], spin components [10] and unitary operators [20].

Quantum optical systems are particularly well suited to address diverse quantum phenomena, such as decoherence and entanglement. However, there is one caveat in the $\Delta x \Delta p_x$ scenario. It is not possible to describe formally the position of photons, usually referred in the literature as spatial localization [21]. The underlying reason being that "There is, strictly speaking, no such a thing as a 'photon wave function' [22, p. 24]". The Riemann-Silberstein vector has been recognized as the most adequate complex mathematical object endowed with most of the required properties [23]. A workaround to photon localization has been to recast the position in terms of the photon energy density [24]. Nonetheless, from an experimental point of view, the problem is much simpler, "A photon is where the photodetector detects it. [25]" It is actually more appropriate to modify the tense "A photon was where the photodetector detected it." because the detection process annihilates the photon.

2. Experimental setup

Two fundamental wave phenomena are exhibited by first order interference, beating and interference fringes. These two manifestations correspond to the perturbances superposition in the temporal or spatial domain. In optical interference fringe setups, the beams are usually derived from the same source. In contrast, temporal interference is commonly achieved with two sources having different frequencies. In this experiment, both phenomena, beating and fringes are simultaneously observed. To this end, we used two carefully stabilized continuous wave Nd:YAG monomode laser sources, with coherence time greater than 300 ns [26]. Highly attenuated 50 ns segments of these beams were isolated with an acousto optic modulator (AOM) and their superposition observed with a streak camera.

2.1. Light sources

The experimental setup in order to measure the position and momentum of the photon ensemble is shown in Fig. 1. The two lasers are truly independent, not even a common trigger is used since the CW beams are obturated after emission. This feature was necessary to insure that their superposition could be represented as a two mode factorizable state in a welcher-weg experiment [27]. The stringent stability conditions in order to observe spatio-temporal interference were met as follows. Two intracavity frequency doubled 50 mW monomode Nd:YAG lasers (AOTK 532Q) were used with reported coherence length larger than 100 m and long term pointing stability better than 10^{-5} rad [26]. The internal temperature control was disconnected in order to take full control externally. The temperature of each laser was monitored with a 100 Ω platinum resistance. Each laser was independently controlled with a Peltier module attached to its base. A temperature controller (SRC10) provided the electronic feedback to maintain a stable temperature within 0.01 °C. The wavelength of each laser was initially monitored with an spectrometer (Spex1704) with 0.1 Å minimum scale resolution ($\triangle\nu$ =12.7 GHz at 5320 Å). The initial wavelengths of the lasers before temperature tunning were $\lambda_{\text{cheb}} = 5317.58 \pm 0.05$ Å and $\lambda_{\text{oxeb}} = 5318.33 \pm 0.05$ Å. Once the frequencies of the two lasers were temperature tuned to overlap in the monochromator measurement, a marginal temperature scan of one laser was performed until fringes were observed in the streak camera (Optronis SC-10). Fluctuations in the lasers wavelengths although tiny, were large enough to produce fringes with different slopes from image to image.

The laser beams were both focused into the same crystal of an acousto optic modulator (AOM) in order to produce 50 ns temporal segments of the CW beams. The AOM uses a TeO_2 crystal with 10/10 ns, 10% to 90% rise/fall time for a 55 μm beam-waist. The AOM first order deflection angle is 25 mrad with a diffraction frequency shift of 210 MHz. One laser beam, codenamed cheb, was incident at normal incidence on the crystal and diffracted in first order (210 MHz). The other laser beam, codenamed oxeb, was incident at 17 mrad approximately on the crystal and operated in second order (2×210 MHz). There was thus a 210 MHz frequency difference that was compensated by the lasers temperature tuning. Half wave retardation plates were used at the output of each laser to adjust the polarization plane in order to improve fringe visibility. A Galilean 10× beam expander was used to increase the beam diameters in order to fill the photocathode detector long axis (8 mm). The beams collimation was adjusted with the aid of a shear interferometer. The two collimated beams are thereafter incident on the streak camera at an angle of 0.14 mrad between them in order to have comfortably resolved interference fringe maxima.

It is not easy to guarantee experimentally that the angle between the two collimated beams is equal and opposite to the normal at the detector's plane. Cartesian coordinates are set with z normal to the detector surface and the fields are linearly polarized in the y direction. Consider two different arbitrary angles α_1, α_2 close to the normal but not necessarily symmetrically opposite to it. Introduce the angle α that bisects these two angles, $\alpha_1 = \alpha - \theta$ and $\alpha_2 = \alpha + \theta$. The wave vectors difference in the x direction is then $\delta k_x = k_{x2} - k_{x1} = \delta k \sin\alpha \cos\theta + 2\bar{k} \cos\alpha \sin\theta$. Since angles are small, approximating the cosines to first order, $\delta k_x \approx \delta k \sin\alpha + 2\bar{k} \sin\theta$. Additionally, the wavevector magnitudes are very similar, thus $\delta k \ll 2\bar{k}$. For example, at an angular frequency difference of $\triangle\omega = 1$ GHz, $\omega_1 + \omega_2 \approx 2 \times 3.542 \times 10^{15}$ Hz, gives a quotient $\frac{\delta k}{2\bar{k}} = \frac{\triangle\omega}{2\omega} \approx 1.411 \times 10^{-7}$. The wave vectors dif-

ference in the x direction is then $\delta k_x \approx 2\bar{k}\sin\theta$, independent of α. In the z direction, $\delta k_z = k_{z2} - k_{z1} = \delta k\cos\alpha\cos\theta - 2\bar{k}\sin\alpha\sin\theta$. Approximating the cosine factors to one, the spatially dependent interference argument evaluated at the plane $z = z_0$ is $\delta\mathbf{k}\cdot\mathbf{r} = 2\bar{k}\sin\theta\, y + \left(\triangle k - 2\bar{k}\sin\alpha\sin\theta\right) z_0$. Thus, if the incidence of the two beams is not symmetrical with respect to the normal, only the phase term in the z direction is significantly modified for small angles. However, in our experiment, this term is constant and does not affect the fringes slope.

2.2. Time and space resolved detection

A streak camera is an optical version of a multichannel electronic oscilloscope. At the entrance slit, light falls on a photocathode (8 mm x 2 mm in the x and y directions respectively) placed on the inner part of a vacuum tube. A photoelectron is emitted at the streak camera photocathode if a photon is present at (x, t). The photo-electrons are swept in the y direction, perpendicular to the long axis. In this way, a two dimensional position versus time image is produced.

At sweep speeds of 10 ns/mm with the TSU-12-10 unit, fringes are observed in the streak camera for frequency differences between the two laser sources below 1 GHz. There are two perpendicular slits at the streak camera entrance. In the y direction, the slit is barely opened at $\delta y = 15$ µm to allow for maximum temporal resolution. The temporal sweep is performed in the y direction with 0.34% resolution of the full sweep time. In the x direction, the slit can be varied from 0 to 15 mm. The input optics, located just after the slits, focuses the image at the photocathode with a $\frac{1}{2}$ de-magnification. The low noise photocathode has dark counts of $100\, e^-/\text{cm}^2\,\text{s}$ (Photek ST-LNS20 with $\times 2.03$ magnification). A photoelectron is emitted with $s = 10.37\%$ quantum efficiency at the streak camera photocathode. The photo-electrons are accelerated and swept in the perpendicular direction to the photocathode long axis. The image formed when the electrons reach the first phosphor screen is amplified via a multichannel plate and thereafter steered by a fiber tapper (25/11.5) to the CCD (Anima-PX/25, 19.5 x 14.9 mm^2, 12 bit A/D, 1392 $\times$ 1024 pixels). Spatial and temporal resolution at the screen are 70 µm and 66 µm, respectively. The reported distances correspond to the coordinates at the device input plane, which are twice as large as those on the photocathode due to the input optics demagnification. This scaling does not alter the $\Delta x\,\Delta p_x$ products because as the distance is halved, the momentum, via the inverse of the slope, is doubled.

Streak images cannot be accumulated in this experiment because the frequency and relative phase between the two lasers vary stochastically from sweep to sweep. For this reason, the fringe pattern was recorded in single exposures with a time duration (50 ns) well below the coherence time (300 ns). Single shot measurements by spectral phase interferometry and ultrashort pulses have also been successfully reported for other purposes [28]. A 3 Hz acquisition repetition rate was used to store the digital images in real time. The beams attenuation and the MCP gain was adjusted to attain, on average, one record per bin at the most. Images with only two levels of gray (black/white) are then noisy but evince the discrete nature of the fields. Recordings at much higher intensities with 256 levels of gray produce smoother images and reduce the noise dramatically but the discrete nature of the phenomenon is no longer evident.

3. Quantum photo detection probability

The quantum field representation of the two electric field operators with linear polarization and positive frequency part are $\hat{E}_1^{(+)}(\mathbf{r}) = i\mathcal{E}_1^{(1)}\exp(i\,\mathbf{k}_1\cdot\mathbf{r})\,\hat{a}_1$ and $\hat{E}_2^{(+)}(\mathbf{r}) = i\mathcal{E}_2^{(1)}\exp(i\,\mathbf{k}_2\cdot\mathbf{r})\,\hat{a}_2$. The one-photon amplitudes are $\mathcal{E}_1^{(1)}$, $\mathcal{E}_2^{(1)}$ and $\hat{a}_1$, $\hat{a}_2$ are the annihilation operators for modes 1 and 2 respectively [29]. The quantum photo detection probability is $w(\mathbf{r},t) = s\langle\psi_{1,2-qc}(t)|\,\hat{E}^{(-)}(\mathbf{r})\,\hat{E}^{(+)}(\mathbf{r})\,|\,\psi_{1,2-qc}(t)\rangle$, where $\hat{E}^{(-)}(\mathbf{r})$ is the Hermitian conjugate of $\hat{E}^{(+)}(\mathbf{r})$. The photo detection interference is

$$w(\mathbf{r},t) = s\left(\mathcal{E}_1^{(1)}\mathcal{E}_2^{(1)}\right)^2\left(\alpha_1\alpha_1^* + \alpha_2\alpha_2^* + \alpha_1^*\alpha_2 \times \exp\left[i\left((\mathbf{k}_2-\mathbf{k}_1)\cdot\mathbf{r} - (\omega_2-\omega_1)\,t\right)\right] + c.c.\right). \tag{1}$$

The photon beams with frequencies ω_1 and ω_2 propagate paraxially to the z direction, at a small but opposite angle of $\theta \approx 0.07$ mrad in the $(\hat{\mathbf{e}}_x, \hat{\mathbf{e}}_z)$ plane. Their wave vectors are $\mathbf{k}_1 = \mathbf{k}_{x1} + \mathbf{k}_{z1} = -\bar{k}\sin\theta\,\hat{\mathbf{e}}_x + \bar{k}\cos\theta\,\hat{\mathbf{e}}_z$ and $\mathbf{k}_2 = \mathbf{k}_{x2} + \mathbf{k}_{z2} = \bar{k}\sin\theta\,\hat{\mathbf{e}}_x + \bar{k}\cos\theta\,\hat{\mathbf{e}}_z$, respectively. The phase of the interference term as a function of the transverse distance x and time t is

$$\phi = 2\bar{k}\sin\theta\, x + \delta k\cos\theta\, z_0 - \delta\omega\, t, \tag{2}$$

where $2\bar{k} = k_1 + k_2$, $\delta k = k_2 - k_1$ and $\delta\omega = \omega_2 - \omega_1$. To avoid confusion, lower case δ is used for differences between the two modes and capital Δ is utilized exclusively for uncertainties. Since the fields superposition is observed at a detector placed at the $z = z_0$ plane, the term $\delta k\cos\theta\, z_0$, only adds a constant phase shift. When the two frequencies are different, the constant phase surfaces evolve in both, time and space. In contrast, constant wavefronts in frequency degenerate setups entail spatial coordinates alone. The slope of the equal-phase planes is

$$\frac{dx}{dt} = \frac{\delta\omega}{2\bar{k}\sin\theta}. \tag{3}$$

The fringes are therefore displaced in time with a velocity $\frac{dx}{dt}$. The photon momentum in the x direction for mode 2 is

$$p_x\,\hat{\mathbf{e}}_x = \hbar\mathbf{k}_{x2} = \hbar\frac{\delta\omega}{2}\left(\frac{dx}{dt}\right)^{-1}\hat{\mathbf{e}}_x, \tag{4}$$

whereas the photon momentum for mode 1 has the opposite sign, $\hbar\mathbf{k}_{x1} = -\hbar\mathbf{k}_{x2}$. The frequency difference $\delta\omega$ and the fringes slope are measurable from experiment, thus the p_x photon momentum can be readily evaluated in this way. The momentum uncertainty written in terms of the maximum and minimum slopes is

$$\Delta p_x = \hbar\frac{\delta\omega}{2}\left(\frac{\left(\frac{dx}{dt}\right)_{\max} - \left(\frac{dx}{dt}\right)_{\min}}{\left(\frac{dx}{dt}\right)_{\max}\left(\frac{dx}{dt}\right)_{\min}}\right). \tag{5}$$

Thus, the momentum uncertainty is proportional to the uncertainty in the slope $\left(\frac{dx}{dt}\right)_{\max} - \left(\frac{dx}{dt}\right)_{\min}$.

4. Experimental rationale and results

A streak camera single shot image of the interference between the two modes with different directions is shown in Fig. 2. The fringes slope would be zero (horizontal) if the two photon beams had the same frequency and infinite (vertical) if the two beams had the same wave vector direction. The inclination reveals that they have different frequency and their wave vectors are not parallel.

Each point in the streak camera image, either bright or dark, represents a quantum test. This test establishes whether a photon arrived at position x of the photocathode at a given time t. Individual and sequential quantum tests are discussed at length in [30, p. 27, p. 237]. Each streak camera image involves two sets of

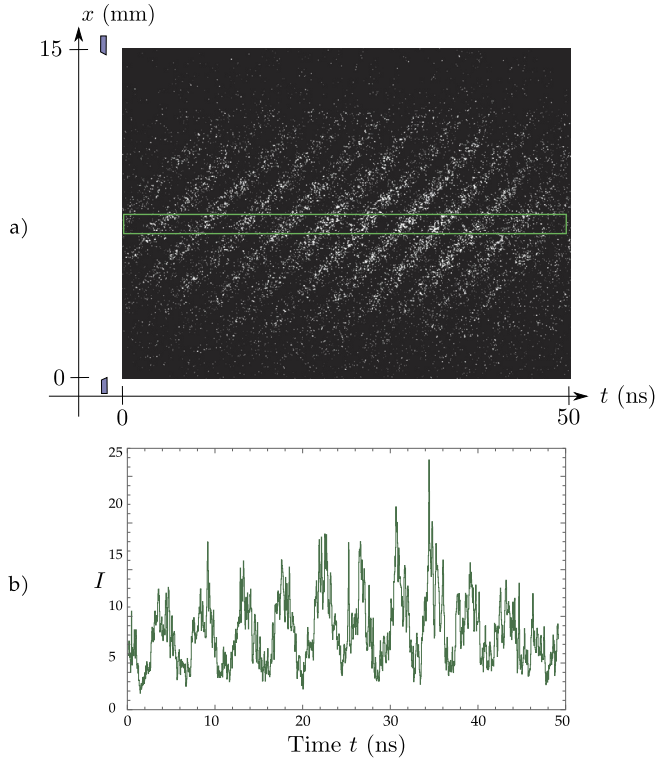

Fig. 2. a) The streak camera image records the photons that hit the detector array as a function of position (ordinate) and time (abscissas). b) The time dependence of the number of photons (proportional to the intensity I in a.u.) is obtained from the spatial average of the region of interest (ROI), drawn in green. The beat frequency between modes $\delta\omega$, is obtained from this plot. Signal is noisy because highly attenuated photon beams with a few number of photons per nanosecond were used.

quantum tests: one in the spatial domain and another in the temporal domain. In the x direction, the electrons in the photocathode long axis act as a set of spatially distributed detectors. For each x position, there is another set of consecutive quantum tests that probe the dynamical evolution of the quantum system. This set is depicted in the abscissas time axis. These events are amplified by the MCP and recorded in the $1024 \times 1392 = 1.425 \times 10^6$ detectors at the CCD. Thus, each streak camera interferogram comprises 10^6 quantum trials (order of magnitude).

The temporal dependence of the number of photons is obtained if their number is summed up in a small spatial region and plotted as a function of time. This ROI is depicted in green in Fig. 2. The corresponding graph exhibits the beating of the two frequencies. From this set of sequential quantum tests, the frequency difference is $\delta\omega = 717 \pm 19$ MHz.

The outcome of the quantum tests when the input slit is fully opened to encompass the region where interference takes place, is shown in Fig. 3. The position uncertainty is $\Delta x = 9.31 \times 10^{-3}$ m. Let us reflect on the meaning of this assertion. In the prevailing Copenhagen view of quantum mechanics, or its modern quantum Bayesian version, the theory is intrinsically probabilistic [31]. A prediction can only be related to observation in an statistical way given by Born's rule. At a given time t, the prediction of where the next photon will be detected, is given by Eq. (1), the quantum photo detection probability $w(x,t)$. The photon's position x is restricted by the detector dimensions, the slit width Δx in this case. From the experimenter point of view, the next photon may fall anyplace within the slit aperture Δx. The fish-tail hard aperture (streak camera input slit) or the equivalent masking of the recorded data, establish Δx in this experiment. Thus, the position observation (preparation) is inside the finite interval of length Δx with probability 1, as required in [32]. By probability 1, what is

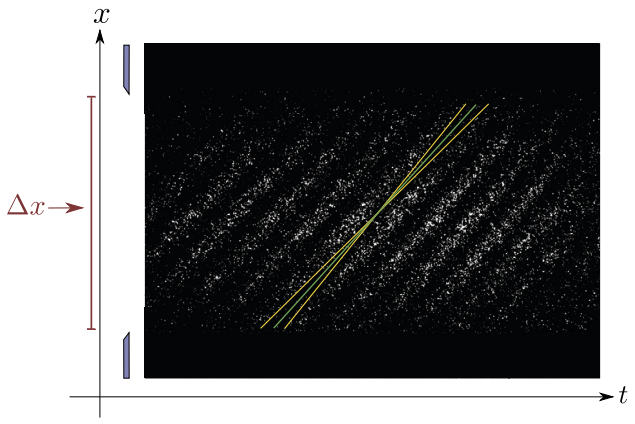

Fig. 3. The input slit of the steak camera is wide opened to 10.12 mm. The fringes slope is unmistakable and its uncertainty is small (max-min yellow slopes). $\Delta x = 9.31 \times 10^{-3}$ m and $\Delta p_x = \hbar \times 1.211 \times 10^2$ m^{-1}, the uncertainty is $\Delta x \Delta p_x = 1.128\hbar > \frac{\hbar}{2}$.

meant is that all the detected photons lie within Δx (almost a tautology). In terms of a distribution function, the overall width Δx is being measured [33, p. 933]. Photons outside Δx are irrelevant, furthermore, recall that non detected photons are not spatially localized.

The momentum uncertainty Δp_x is directly proportional to the difference of the maximum and minimum slopes (5). The slopes extrema were drawn by hand prior to any $\Delta x \Delta p_x$ calculation to avoid any bias. An arbitrary dark fringe was chosen and parallel slopes to the median were drawn (the distance between them was roughly half the distance between fringe maxima). The slopes extrema were obtained from the diagonals of the parallelogram. Their coordinates were obtained from the tooltips of the digital recordings.

The fringes slope (green in Fig. 3) is $\frac{dx}{dt} = 0.449$ mm/ns, whereas the maximum and minimum slopes (in yellow) are $\left(\frac{dx}{dt}\right)_{\max} = 0.499$ mm/ns and $\left(\frac{dx}{dt}\right)_{\min} = 0.427$ mm/ns respectively. The momentum, from (4) is

$$p_x \hat{\mathbf{e}}_x = \hbar \times 7.987 \times 10^2 \text{ m}^{-1}\, \hat{\mathbf{e}}_x.$$

From the minimum and maximum slopes, the maximum and minimum momenta are $p_{x\text{-max}} = \hbar \times 8.398 \times 10^2$ m^{-1}, $p_{x\text{-min}} = \hbar \times 7.187 \times 10^2$ m^{-1} respectively. The momentum uncertainty is obtained from their difference, $\Delta p_x = \hbar \times 1.211 \times 10^2$ m^{-1}. The product of uncertainties is

$$\Delta x \, \Delta p_x = \left(9.31 \times 10^{-3}\right) \times \left(\hbar \times 1.211 \times 10^2\right) = 1.128\hbar > \frac{\hbar}{2}.$$

The measured $\Delta x \Delta p_x$ is 2.26 times the minimum achievable quantum uncertainty. Let us compare these results with the device's accuracy. The instrumental position resolution is $\Delta x_{\text{inst}} = 70$ µm, well beyond the photons position spread. At 2.5 ns/mm sweep speed, the temporal resolution is 0.2 ns, where from, the momentum instrumental resolution for a 0.449 mm/ns slope, is $\Delta p_{x\,\text{inst}} = \hbar \times 0.284 \times 10^2$ m^{-1}. This value is four times smaller than the quantum momentum uncertainty Δp_x. Therefore, it is clear that *the photons position and momentum predominant uncertainties, do not arise from the instrumental resolution but are due to the quantum nature of the system.*

If the input slit is limited to a smaller aperture, the photon positions are restricted to a smaller $\Delta x = 2.01 \times 10^{-3}$ m interval as shown in Fig. 4. This result is equally obtained if the streak camera image is masked in the x axis to the corresponding Δx range. The fringes slope (in green) is $\frac{dx}{dt} = 0.404$ mm/ns, where from

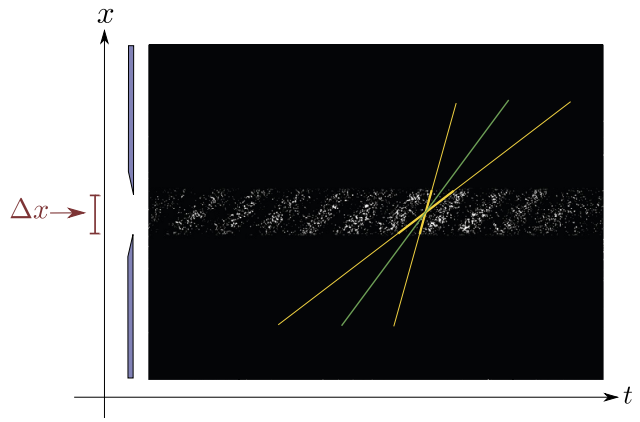

Fig. 4. The position spread Δx is reduced to ≈ 2 mm (ordinate axis). The fringes slope is still noticeable but the maximum and minimum slopes (in yellow) interval is widened. The position uncertainty becomes sharper but the momentum is less well defined. $\Delta x = 2.01 \times 10^{-3}$ m and $\Delta p_x = \hbar \times 1.227 \times 10^3$ m^{-1}, the uncertainty is $\Delta x \, \Delta p_x = 2.464 \hbar > \frac{\hbar}{2}$.

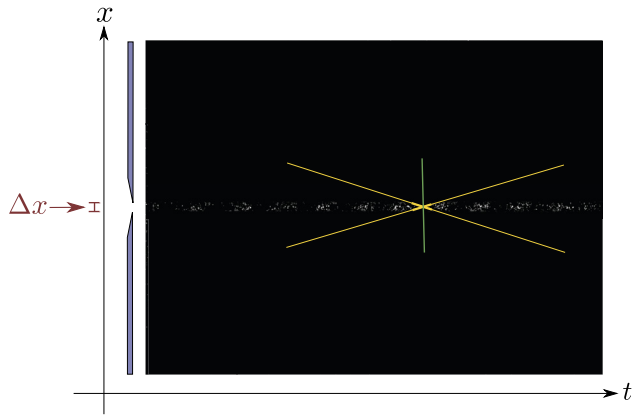

Fig. 5. The position spread Δx is further reduced to 0.36 mm. The fringes slope is 'guessed' in green with the maximum and minimum slopes depicted in yellow. The inclination of the fringes is not discernible.

$p_x \hat{\mathbf{e}}_x = \hbar \times 8.876 \times 10^2$ m^{-1} $\hat{\mathbf{e}}_x$. From the slopes extrema, the maximum and minimum momenta are $p_{x\text{-max}} = \hbar \times 15.660 \times 10^2$ m^{-1} and $p_{x\text{-min}} = \hbar \times 3.383 \times 10^2$ m^{-1}. The momentum uncertainty is $\Delta p_x = \hbar \times 12.277 \times 10^2$ m^{-1} and the product of uncertainties is

$$\Delta x \, \Delta p_x = \left(2.01 \times 10^{-3}\right) \times \left(\hbar \times 12.277 \times 10^2\right) = 2.464 \hbar > \frac{\hbar}{2}.$$

The position uncertainty was reduced but there was a momentum uncertainty increase consistent with Heisenberg's principle. Notice that the decrease/increase of the complementary variables uncertainties is directly visualized from the experimental results.

If the spatial spread is further reduced, regions with a high and low density of photon specks are observed as a function of time (see Fig. 5). Namely, the beating where from the energy difference was obtained from the rectangular ROI in Fig. 2. However, we can hardly speak of a momentum measurement since it is a wild guess what the slope is and the slope uncertainty is huge. Nonetheless for the slope (in green) the momentum is $p_x \hat{\mathbf{e}}_x = \hbar \times 4.34 \times 10^1$ m^{-1} $\hat{\mathbf{e}}_x$. The momentum uncertainty $\Delta p_x = \hbar \times 7.65 \times 10^3$ m^{-1} is much larger than p_x, so that $p_x \pm \Delta p_x/2$ can even be either positive or negative. The position spread is $\Delta x = 3.56 \times 10^{-4}$ m. The uncertainty relationship is

$$\Delta x \, \Delta p_x = \left(0.356 \times 10^{-3}\right) \left(\hbar \times 76.5 \times 10^2\right) = 2.7 \hbar > \frac{\hbar}{2}.$$

Again, the position uncertainty is further reduced but the momentum uncertainty becomes even larger.

Notice that the position sharpness does not hinder the precision in the energy measurement. The energy difference between the two modes $\mathcal{E} = \hbar \, \delta\omega = \hbar \times (7.17 \pm 0.19) \times 10^8$ Hz, was evaluated from the time vs. intensity graph in Fig. 2. We could in fact, extend the time measurement (longer sweep times) to improve the precision in $\mathcal{E}$ while keeping Δx very small. Since x does not vary in time within the observed segment for a given z_0, it commutes with the Hamiltonian $\frac{dx}{dt} = \frac{i}{\hbar}[\mathcal{H}, x] = 0$, thus, position x and energy can both be evaluated to arbitrary precision.

5. Discussion and conclusions

This experiment demonstrates that it is actually possible to perform a joint measurement of position and momentum in an ensemble, in this case a 9 mm spatial region with 50 ns time span. Quantitatively, the $\Delta x \, \Delta p_x$ reported uncertainties are $1.128\hbar$, $2.464\hbar$ and $2.723\hbar$. Similar outcomes were obtained from many other measurements. The larger values compared with the $0.5\hbar$ quantum limit are likely to be due to an over estimate of the max-min slopes values. This result is not surprising considering that the slopes extrema were not obtained at one standard deviation but by a crude maximum/minimum geometrical parallelogram method. Some authors have suggested that the uncertainty relationship should be $\Delta x \, \Delta p_x \geq \frac{\hbar}{2}$, that in terms of $\hbar$ is $\Delta x \, \Delta p_x \geq \pi\hbar$ [34,32]. The outcome of our experiments rule out this possibility, provided that our uncertainty estimates are equal or larger than the effective (overall) width of the distribution functions [33], since all reported values in units of $\hbar$ are smaller than π.

In the classical limit, ostensibly no uncertainty is present since $\lim_{\hbar \to 0} \left\{ \Delta x \, \Delta p_x \geq \frac{\hbar}{2} \right\} = \Delta x \, \Delta p_x \geq 0$. However, recall that the photon linear momentum is $\hbar \mathbf{k}_x$, so that $\lim_{\hbar \to 0} \left\{ \Delta x \hbar \Delta k_x \geq \frac{\hbar}{2} \right\} = \Delta x \, \Delta k_x \geq \frac{1}{2}$ is non zero even in the classical limit. The uncertainty persists due to the wave nature of the electromagnetic fields, and hence the widths of Fourier transform pairs, is still present in the classical limit. An altogether different case would arise if the product of the photon number - phase uncertainties product $\sqrt{\langle N_\ell \rangle} \Delta\phi$ were considered. Fock states have a well defined photon number but interference is not describable in terms of these states because the phase is random. Coherent states are commonly used in quantum optics in order to describe quantum interference, but then the photon number is not well defined. For minimum uncertainty states and in particular for coherent states, the number of photons N_ℓ is described by a Poisson distribution [29, p. 368]. If we measure the total number of photons (spots on the interferograms) in different images, these values, for a large number of images, should have the form of a Poisson distribution. In the limit of macroscopic fields and small quantum fluctuations, N_ℓ and the phase ϕ_ℓ fluctuations look like complementary variables $\triangle N_\ell \triangle \phi_\ell \geq \frac{1}{2}$. But let us insist, this number is not relevant for the $\Delta x \Delta p$ evaluation as long as there are enough photons to distinguish the fringes.

The position and momentum are being measured in coordinate space, that is where we live. For this reason, each detected photon can be localized at a point in (x, t). Momentum, the complementary variable, requires a large set of photons to establish its value (slope). In momentum space, the converse applies, the momentum of each photon is known but an ensemble is needed to establish their position. In the present experiment, the ensemble measurement is performed in a Δx region (0.3 to 9.3 mm) for a very short duration, namely 50 ns. In this space-time interval, the position and momentum of the ensemble were jointly measured.

CRediT authorship contribution statement

M. Fernández Guasti: Writing – review & editing, Writing – original draft, Methodology, Investigation, Funding acquisition, Formal analysis, Conceptualization.

Declaration of competing interest

The authors declare that they have no known competing financial interests or personal relationships that could have appeared to influence the work reported in this paper.

Data availability

Data will be made available on request.

Acknowledgement

We acknowledge support by CONACYT, projects CB2005-51345-F-24696 and CB2010-151137-F.

References

[1] S. Capozziello, W.G. Boskoff, A Mathematical Journey to Quantum Mechanics, Springer, 2021.
[2] P.W. Lamberti, G.M. Bosyk, S. Fortin, F. Holik, Quantum Foundations, 2019.
[3] V. Jijnasu, The uncertainty principle – a simplified review of the four versions, Stud. Hist. Philos. Sci. Part B, Stud. Hist. Philos. Mod. Phys. 55 (2016) 62–71.
[4] R. Penrose, Uncertainty in quantum mechanics: faith or fantasy?, Philos. Trans. R. Soc. A, Math. Phys. Eng. Sci. 369 (2011) 4864–4890.
[5] W. Heisenberg, Uber den anschaulichen inhalt der quantentheoretischen Kinematik und Mechanik, Z. Phys. 43 (1927) 172–198.
[6] E.H. Kennard, Zur quantenmechanik einfacher Bewegungstypen, Z. Phys. 44 (1927) 326–352.
[7] M. Ozawa, Universally valid reformulation of the Heisenberg uncertainty principle on noise and disturbance in measurement, Phys. Rev. A 67 (2003) 042105.
[8] J. Erhart, S. Sponar, G. Sulyok, G. Badurek, M. Ozawa, Y. Hasegawa, Experimental demonstration of a universally valid error–disturbance uncertainty relation in spin measurements, Nat. Phys. 8 (2012) 185–189.
[9] L.A. Rozema, A. Darabi, D.H. Mahler, A. Hayat, Y. Soudagar, A.M. Steinberg, Violation of Heisenberg's measurement-disturbance relationship by weak measurements, Phys. Rev. Lett. 109 (2012) 100404.
[10] W. Ma, B. Chen, Y. Liu, M. Wang, X. Ye, F. Kong, F. Shi, S. Fei, J. Du, Experimental demonstration of uncertainty relations for the triple components of angular momentum, Phys. Rev. Lett. 118 (2017) 180402.
[11] C.G. Shull, Single-slit diffraction of neutrons, Phys. Rev. 179 (1969) 752–754.
[12] O. Nairz, M. Arndt, A. Zeilinger, Experimental verification of the Heisenberg uncertainty principle for fullerene molecules, Phys. Rev. A 65 (2002) 032109.
[13] D. Nikolic, L. Nesic, Verification of the uncertainty principle by using diffraction of light waves, Eur. J. Phys. 32 (2011) 467–477.
[14] M.J. Mobley, Momentum exchange theory of photon diffraction, Opt. Eng. 57 (2018) 1.
[15] P. Busch, T. Heinonen, P. Lahti, Heisenberg's uncertainty principle, Phys. Rep. 452 (2007) 155–176.
[16] J.W. Noh, A. Fougères, L. Mandel, Measurement of the quantum phase by photon counting, Phys. Rev. Lett. 67 (1991) 1426–1429.
[17] G. Breitenbach, S. Schiller, J. Mlynek, Measurement of the quantum states of squeezed light, Nature 387 (1997) 471–475.
[18] M. Beck, C. Dorrer, I.A. Walmsley, Joint quantum measurement using unbalanced array detection, Phys. Rev. Lett. 87 (2001) 253601.
[19] M. Ringbauer, D.N. Biggerstaff, M.A. Broome, A. Fedrizzi, C. Branciard, A.G. White, Experimental joint quantum measurements with minimum uncertainty, Phys. Rev. Lett. 112 (2014) 020401.
[20] L. Xiao, K. Wang, X. Zhan, Z. Bian, J. Li, Y. Zhang, P. Xue, A.K. Pati, Experimental test of uncertainty relations for general unitary operators, Opt. Express 25 (2017) 17904.
[21] O. Keller, On the theory of spatial localization of photons, Phys. Rep. 411 (2005) 1–232.
[22] M.O. Scully, M.S. Zubairy, Quantum Optics, CUP, 2001.
[23] M. Elbistan, P.A. Horváthy, P.M. Zhang, Duality and helicity: the photon wave function approach, Phys. Lett. A (2017) 2375–2379.
[24] I. Bialynicki-Birula, Z. Bialynicka-Birula, Uncertainty relation for photons, Phys. Rev. Lett. 108 (2012) 140401.
[25] A. Muthukrishnan, M.O. Scully, M.S. Zubairy, The concept of the photon - revisited, in: Optics and Photonic News, OSA, 2003, pp. S18–S27.
[26] M. Fernández-Guasti, H. Palafox, R. Chandrasekar, Coherence and frequency spectrum of a Nd: YAG laser - generation and observation devices, in: Optics and Photonics 2011, in: The Nature of Light: What Are Photons? IV, vol. 8121, SPIE, 2011, 81211E-1-10.
[27] M. Fernández-Guasti, C. García-Guerrero, Time and space resolved first order optical interference between distinguishable photon paths, Front. Phys. 9 (2022) 1–10.
[28] T. Akagawa, K. Misawa, R. Lang, Single-shot phase measurement by spectral phase interferometry using a streak camera, in: 14th International Conference on Ultrafast Phenomena, OSA, 2004, p. TuE22.
[29] G. Grynberg, A. Aspect, C. Fabre, Introduction to Quantum Optics, CUP, 2010.
[30] A. Peres, Quantum Theory: Concepts and Methods, Fundamental Theories of Physics, vol. 72, Kluwer Academic, 2002.
[31] L.E. Ballentine, The statistical interpretation of quantum mechanics, Rev. Mod. Phys. 42 (1970) 358–381.
[32] T. Schürmann, I. Hoffmann, A closer look at the uncertainty relation of position and momentum, Found. Phys. 39 (2009) 958–963.
[33] J.B.M. Uffink, J. Hilgevoord, Uncertainty principle and uncertainty relations, Found. Phys. 15 (1985) 925–944.
[34] P. Millette, The Heisenberg uncertainty principle and the Nyquist-Shannon sampling theorem, Prog. Phys. 3 (2013).